A Study on Heat Source Equations for the Prediction of Weld Shape and Thermal Deformation in Laser Microwelding

W.-S. CHANG and S.-J. NA

In the area of laser welding, numerous studies have been performed in the past decades using either analytical or numerical approaches, or both combined. However, most of the previous studies were process oriented and modeled conduction and keyhole welding differently. In this research, various heat source equations that have been proposed in previous studies were calculated and compared with a new model. This is to address the problem of predicting, by numerical means, the thermomechanical behavior of laser spot welding for thin stainless steel plates. A finite-element model (FEM) code, ABAQUS, is used for the heat transfer and mechanical analysis with a three-dimensional plane assumption. Experimental studies of laser spot welding and measurement of thermal deformation have also been conducted to validate the numerical models presented. The results suggest that temperature profiles and weld deformation vary according to the heat source equation of the laser beam. For this reason, it is essential to incorporate an accurate model of the heat source.

I. INTRODUCTION

LASER welding has become a significant industrial process because there are many outstanding advantages in using laser welding over other widely used bonding technologies. As an alternative to the common adhesives or solders used for the joining process, laser welding offers a number of attractive features such as high weld strength to weld size ratio, reliability, and minimal heat-affected zone. These provide the benefits of low heat distortion, a noncontact process, repeatability, ability to automate, and high throughput. For these reasons, the applications of laser beam welding have broadened in the past decades.

Concurrently, the need to predict laser welding behavior has also become more important since thermal analysis of the laser weld joint is a prerequisite for designing the process parameters as well as the mechanical attributes of the joint, *i.e.*, the thermal distortion and residual stresses. Studies have shown that the laser welding process is very complex, including such phenomena as thermal conduction in a multiphase system, fluid flow, gas dynamics, and plasma effects. A number of simple analytical and numerical models have been developed to describe various aspects of the laser welding process, usually for a specific range of conditions where one or a few phenomena dominate the process.[1,2,3] For this reason, sophisticated computational models of laser welding are required to study a wider range of conditions and the mutual interactions among the various phenomena, although the analysis requires a great deal of calculation.

More complicated models and much more computationally intensive calculations become possible as computer technology develops. The model to be described here was designed to extend the capabilities of numerical analysis using the heat source equation to a wide range of process conditions. It especially concerns laser spot welding of thin plates, which is usually used for small-parts joining processes. In this study, numerical analyses, which use previous heat source equations, and those that use the proposed one are performed and compared with each other. Experimental studies of laser spot welding have also been conducted to validate the numerical models presented. Numerical analyses are performed using a commercial FEM code, ABAQUS.

W.-S. CHANG, Senior Research Scientist, is with the Nano Process Group, Korea Institute of Machinery and Material, Daejeon 305-343, Korea. Contact e-mail: paul@kimm.re.kr S.-J. NA, Professor, is with the Department of Mechanical Engineering, Korea Advanced Institute of Science and Technology, Daejeon 305-701, Korea.

Manuscript submitted July 25, 2001.

A. *Previous Model of Laser Welding*

Mazumder and Steen[3] developed the first numerical model of the continuous laser welding process. This model implemented the finite-difference technique for a Gaussian beam intensity distribution and started with the assumption that the laser beam source is treated as heat flux and the absorptivity of the incident radiation below the boiling point was 20 pct but the absorptivity of laser radiation was considered to be 100 pct when the temperature exceeded the boiling point. They also assumed that the energy absorption followed the Beer–Lambert's law, $q_z = q_0 e^{-\beta z}$, where β is the absorption coefficient and q_z and q_0 are the intensities at depth z and on the surface, respectively. This model may simulate the physical phenomena of the initiation of the keyhole. Zacharia *et al.*[4,5] also developed a two-dimensional finite-difference model using a Gaussian heat-flux equation to describe the convective flow and heat transfer in the fusion zone. A Gaussian heat flux $Q(r)$ is presented as follows:

$$Q(r) = \frac{3P}{\pi \overline{r_1}^2} \exp\left(-3\,\frac{r^2}{\overline{r_1}^2}\right) \qquad [1]$$

where the effective radius $\overline{r_1}$ is assumed at which the intensity falls to 5 pct of the peak value and total optical power (P) by the laser beam is the integral of the optical intensity over a transverse plane (say, at a distance z),

$$P = \int_0^\infty I(r, z) 2\pi r dr \qquad [2]$$

The model of Mazumder *et al.* was combined with a heat-flux equation and used as internal heat generation in the

case of deep penetration welding.[6,7] The combined heat source equation is presented as follows:

$$Q(r, z) = \frac{2\beta P}{\pi \overline{r_2}^2} \exp\left(-2\frac{r^2}{\overline{r_2}^2} - \beta z\right) \quad [3]$$

where the effective radius $\overline{r_2}$ is assumed at which the intensity falls to 13.5 pct of the peak value. Sonti and Amateau[8] also treated the laser weld heat input as an internal heat source rather than a surface flux by using the relation

$$Q(r, z) = \frac{9P}{\pi \overline{r_3}^2 \overline{z}} \exp\left(-3\frac{r^2}{\overline{r_3}^2} - 3\frac{z}{z}\right) \quad [4]$$

Thus, the heat source was assumed to have a Gaussian distribution in the radial direction with exponential decay in the thickness direction. An effective radius and depth of the energy source, $\overline{r_3}$ and $\bar{z}$, respectively, were assumed at which the intensity falls to 5 pct of the peak value. As another model, it was proposed that the volumetric heat source has a Gaussian transverse distribution, corresponding to the laser intensity profile, and this distribution extends uniformly with depth into the material for a distance d_k, forming a "Gaussian rod,"[9] which is represented as

$$Q(r, z) = \frac{P}{\pi \overline{r_4}^2 d_k} \exp\left(-\frac{r^2}{\overline{r_4}^2}\right) u(z) \quad [5]$$

where the effective radius $\overline{r_4}$ is assumed at which the intensity falls to 37 pct of the peak value, $u(z) = 1$ for $0 \le z \le d_k$, and $u(z) = 0$ otherwise. The distance d_k is the maximum keyhole depth, or maximum penetration of the vaporization isotherm into the material, and must be determined iteratively as part of the model.

B. *The Proposed Heat Source Equation*

Previous heat source equations have been used to solve just the energy balance equation with appropriate initial and boundary conditions. The laser spot welding process is somewhat more complicated than just the simple diffusion of heat away from the surface because of the short process time with high beam intensity. In this study, the mechanism of the propagation of the beam into a material, closely related to the energy balance problem, is considered. In the simplest case, the beam power absorbed locally at the keyhole wall can be described by considering only the Fresnel absorption of the beam intensity distribution $I(x,y,z)$ hitting the surface. The intensity of the laser beam has a Gaussian–like distribution:[10]

$$I(x, y, z) = I(r, z) = I_0(t)\left(\frac{r_{f0}}{\overline{r}_f}\right)^2 \exp\left(-\frac{2r^2}{r_f^2}\right) \quad [6]$$

where I_0 is the beam intensity at the beam's focal point (W/m^2), r_{f0} the beam's focal radius (m), r_f the beam's radius at depth z (m), and r the radial distance from the center of the beam (m). It is determined by the focusing number F of the focusing optics, the wavelength λ, and the beam quality M^2. Whereas an ideal Gaussian TEM_{00} beam has $M^2 = 1$, for real multikilowatt laser beams, a larger value for M^2 must be used. These parameters lead to the focal radius

$$r_{f0} = \frac{2\lambda F M^2}{\pi} \quad [7]$$

and the Rayleigh length (depth of focus):

$$z_r = \pm 2 r_{f0} F \quad [8]$$

with the beam radius $r_f(z)$ varying over the depth by

$$r_f(z) = r_{f0}\left[1 + \left(\frac{z - z_0}{z_r}\right)^2\right]^{1/2} \quad [9]$$

where z_0 is the position of the focal plane relative to the upper surface of the workpiece; in this work, positive values are in the beam direction. The peak intensity I_0 is expressed as follows:

$$I_0 = \frac{2P}{\pi r_{f0}^2} \quad [10]$$

where P is defined in Eq. [2]. The final form of the volumetric heat source term, $Q(x,y,z,t)$, can be expressed as

$$Q(x, y, z, t) = Q(r, z, t) = \frac{2P(t)}{\pi r r_{f0}^2 d}\left(\frac{r_{f0}}{r_f}\right)^2 \exp\left[-\frac{2r^2}{r_f^2}\right] \cdot u(z) \quad [11]$$

where $u(z) = 1$ for $0 \le z \le d$ and $u(z) = 0$ otherwise; d is the beam penetration depth, which is given by the drilling velocity v_d, and r_{f0} and r_f are the beam's focal radius at surface and depth, respectively. At the centerline of the workpiece, the temperature gradient in the transverse direction can be neglected due to symmetry of heat flow. The amount of volumetric heat is determined by beam penetration depth.

C. *Beam Penetration Depth*

For spot welding, there are two main mechanisms for removal of material from the beam interaction zone and consequent propagation of melt front into the metal bulk. They are (1) melt ejection by the vaporization-induced recoil force and (2) melt evaporation. When a high-power beam initially strikes, the surface temperature rapidly reaches the melting point and even boiling point of the material. It induces recoil pressure to the melt surface and makes a small hole known as a keyhole. Semak *et al.*[11,12] made the one-dimensional (1-D) model, which considered the heat transfer due to the recoil pressure induced melt flow. From this model, the three-dimensional (3-D) melt flow model was proposed in this study to calculate the beam penetration velocity or drilling velocity. The 3-D model of the melt layer is shown schematically in Figure 1, in which the R-axis is directed along the spot radius and the Z-axis coincides with the normal to the melt surface. If the steady-state regime of evaporation and melt ejection is reached, then the melting front and the melt-vapor interface propagate inside the material along the Z-axis with velocity v_d, which subsequently is called the "drilling" velocity. The rate of melting of solid metal equals the sum of the melt ejection and evaporation rates, so the mass conservation equation gives

$$\pi r_f^2 \rho_s v_d = 2\pi r_f \delta_m \rho_m v_m + \pi r_f^2 \rho_m v_v \quad [12]$$

where ρ_s and ρ_m are the densities of the solid and liquid

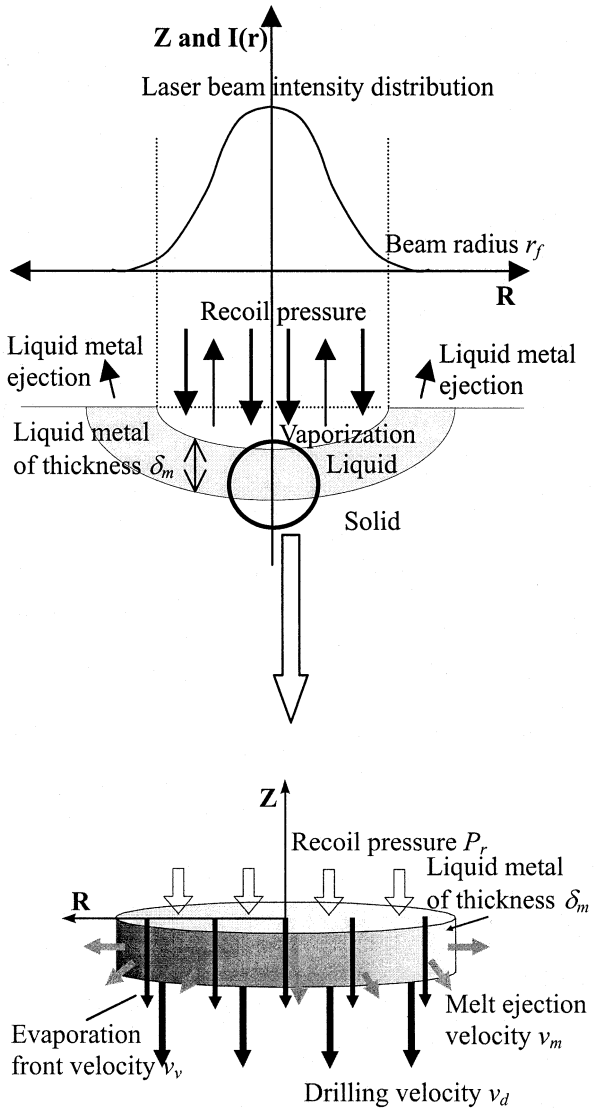

Fig. 1—Physical model of melt removal from the interaction zone.

phases, respectively; δ_m is the melt-layer thickness; v_d is the drilling velocity; v_m is the melt-ejection velocity along the radial direction of the melt layer; and v_v is the evaporation front's velocity directed along the *Z*-axis. As Semak and Matsunawa assumed, the melt thickness (δ_m), during steady-state front propagation with velocity v_d, is approximately calculated as

$$\delta_m \approx a_m / v_d \qquad [13]$$

where a_m is the diffusion coefficient. Then, Eq. [12] is rewritten in the following form:

$$v_d^2 - \frac{\rho_m}{\rho_s} v_v v_d - 2 \frac{\rho_m}{\rho_s} \frac{a_m}{r_f} v_m = 0 \qquad [14]$$

Solving the quadratic Eq. [14] and taking only the positive solution gives

$$v_d = \frac{1}{2} \left[\frac{\rho_m}{\rho_s} v_v + \left\{ \left(\frac{\rho_m}{\rho_s} v_v \right)^2 + 8 \frac{\rho_m}{\rho_s} \frac{a_m}{r_f} v_m \right\}^{1/2} \right] \qquad [15]$$

The value of the evaporation front velocity v_v is determined by the melt's surface temperature T_s:

$$v_v = V_0 \exp(-U/T_s) \qquad [16]$$

where $U = M_a L_v / (N_d k_b)$, M_a is the atomic mass, L_v is the latent heat of evaporation, N_a is Avogadro's number, k_b is Boltzmann's constant, and V_0 is a constant whose value is of the order of the speed of sound in the condensed phase.

The evaporation-induced recoil pressure generates melt flow with the dominant direction being that in which the recoil-pressure gradient is the highest. This means that, in laser welding or drilling, the recoil pressure will provide melt ejection to the sides of the weld pool or cut. Assuming that a steady state has been reached and the melt flow is like a 1-D flow. Thus, Bernoulli's equation was used to relate the melt velocity v_m at the edge of the laser spot to the value of the recoil pressure P_r:

$$v_m = \sqrt{\frac{2P_r}{\rho_m}} \qquad [17]$$

According to the calculations performed by Anisimov and Khoklov,[13] recoil pressure (P_r) is used as follows:

$$P_r = AP_s(T_s) = AB_0 T_s^{-1/2} \exp(-U/T_s) \qquad [18]$$

where P_s is saturated vapor pressure, T_s is the melt's surface temperature, A is a numerical coefficient, B_0 is a vaporization constant, and U is the same as that defined in Eq. [16]. From this relationship, the drilling velocity (v_d) is calculated at each time-step and the beam penetration depth (d) is given as $d = v_d t$.

D. *Governing Equation and Boundary Conditions*

The heat transfer of laser spot welding can be calculated by applying heat conduction theory, and the thermal and mechanical aspects of the problem can be decoupled without imposing a significant penalty on the calculation accuracy. The following assumptions were made in the formulation of the FEM.

(1) The workpiece is initially at 20 °C. Both the laser beam and coordinate mesh are fixed.
(2) All thermophysical properties are considered to be temperature dependent, and above the boiling point, the thermophysical properties for iron vapor at 2860 °C[14] are used.
(3) The latent heat of fusion and vaporization is considered according to Matsuhiro *et al.*[15]
(4) At the surface, absorptivity of 36 pct is assumed,[16] while below the surface, absorptivity of 90 pct, which is induced by multireflection on the internal wall and plasma absorption, is assumed.[17]

The energy equation of the problem is

$$\rho(T) C(T) \frac{\partial T}{\partial t} = \nabla \cdot (K(T) \nabla T) + Q(x, y, z) \qquad [19]$$

where $\rho(T)$ is temperature-dependent density, $C(T)$ is temperature-dependent specific heat capacity, $K(T)$ is temperature-dependent thermal conductivity, and Q is power generation per unit volume in the domain.

The natural boundary condition can be defined by

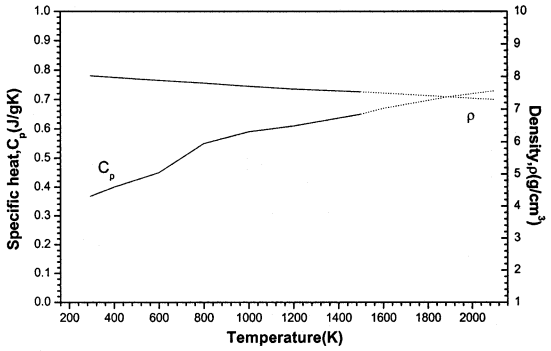

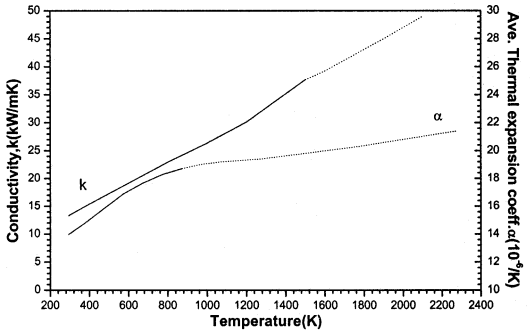

Fig. 2—Temperature-dependent thermal properties.

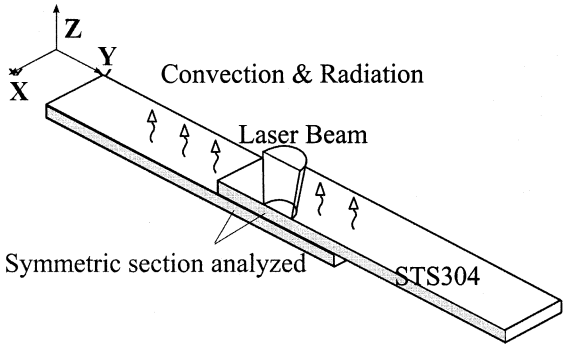

Fig. 3—Symmetric physical model for thermal analysis of laser spot welding.

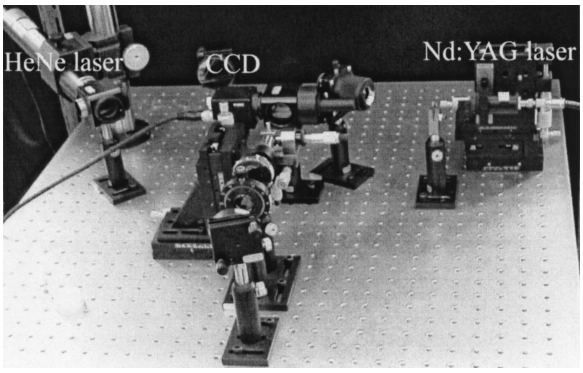

Fig. 4—(*a*) and (*b*) Experimental setup of laser spot welding and ESPI.

$$k_n \frac{\partial T}{\partial n} - q + h(T - T_0) + \sigma\varepsilon(T^4 - T_0{}^4) = 0 \quad [20]$$

where k_n is the thermal conductivity normal to surfaces that are subject to radiation, convection, and imposed heat fluxes; q is the heat flux; h is the heat-transfer coefficient for convection; σ is the Stefan–Boltzmann constant for radiation; and ε is emissivity. The convection coefficient used was $h = 10$ W/m^2 K and the emissivity (ε) value of 0.25 was assumed for stainless steel.[18] The heat flux specified on the workpiece surface is given by incident laser beam. During laser spot welding, heat losses from the workpiece surface are through natural convection, radiation, and evaporation of molten metal. Only the convective and radiative heat losses were applied for this study. The initial condition for the transient analysis is T (x, y, z, 0) = (T_0(x, y, z), where T_0 is the initial temperature.

E. *Material Properties*

As previously noted, the material to be joined is AISI type 304 stainless steel plate. Temperature-dependent thermal properties of this material were assumed to be isotropic and homogeneous and are shown in Figure 2. Since thermal properties over the melting point are not known, linearly extrapolated properties were used in the simulation. The latent heat of fusion was 247 kJ/kg, to be released or absorbed over the temperature range from solidus temperature (T_{Sol}) 1400 °C to liquidus temperature (T_{Liq}) 1500 °C, and the latent heat of vaporization was 7600 kJ/kg.[15]

F. *Description of Discrete Model*

To simulate the pulsed laser spot welding process, a 3-D thermal analysis was used. To consider the temperature-dependent parameters in the formulation of the laser spot welding process, the model relied on solving a nonlinear parabolic differential equation for heat diffusion. The nonlinear finite-element solver, ABAQUS, was employed to solve the transient thermal analysis of the problem.[20] The specimen was taken in the form of two flat plates connected at the joint part. The overall geometry and boundary conditions of the solution domain are shown schematically in Figure 3.

Since the symmetry to the y-axis, as shown in Figure 3, is evident, only half of the plates were modeled, based on eight-node quadratic 3-D solid elements in the finite-element analysis. The mesh size was approximately 90 μm near the centerline of the laser beam at which the temperature gradient is steep. The time-step was controlled according to the criterion that the temperature change between any two adjacent time-steps was less than 500 K. The thermal analysis of one pulse laser spot welding proceeded for 4 seconds when the temperature inside the specimen was expected to cool down to approximately 373 K.

II. EXPERIMENTS

Experiments were designed to evaluate the numerical results. Figure 4 shows the experimental setup of the laser welding system and optical configuration of electronic speckle pattern interferometry (ESPI) used for determining the out-of-plane displacement of optoelectronic components. The basic idea of ESPI is to compare the typical patterns in the image plane before and after the deformation of an object has taken place. Since the individual images are stored electronically in a computer, the handling of such a system is convenient.[21,22] The system consists of a pulse Nd:YAG

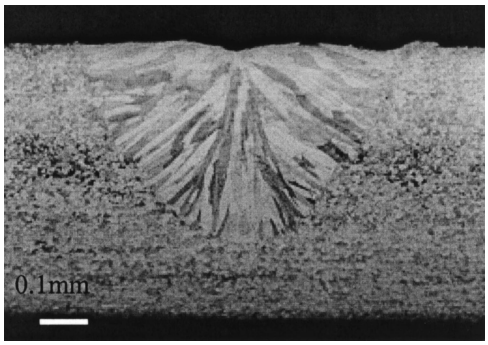

(*a*)

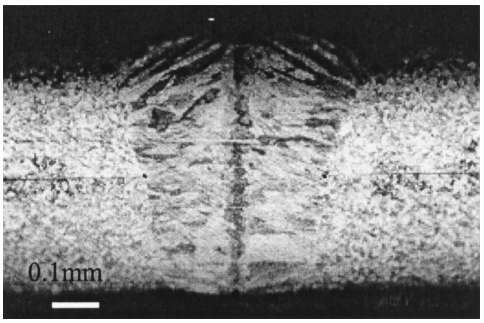

(*b*)

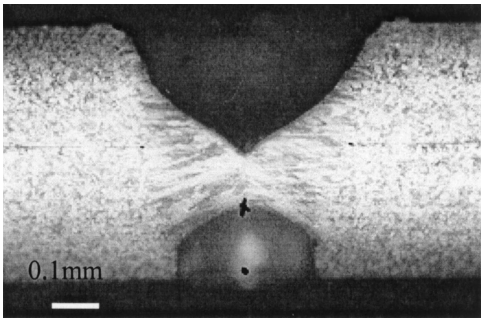

(*c*)

Fig. 5—Morphologies of a sectioned specimen with various conditions: (*a*) energy = 2.5 J, pulse duration = 4 ms, and focal position = +1.0 mm; (*b*) energy = 3.0 J, pulse duration = 4 ms, and focal position = +0.5 mm; and (*c*) energy = 3.5 J, pulse duration = 4 ms, and focal position = +0.5 mm.

laser, a fiber optic beam delivery system, a charge-coupled device (CCD) camera, a HeNe laser, and optics for the speckle interferometer. A laser beam delivered from the Nd:YAG laser to the workpiece is accurately adjusted with a three-axis stage. Type 304 stainless steel specimens, which consist of two sheets with thickness 0.3 and 0.33 mm as shown in Figure 3, were prepared for the experiments. Exposure of a stainless steel sheet to a laser pulse formed a spot weld, which was then sectioned and prepared to measure the fusion zone dimensions. Some typical morphologies of the sectioned specimen are shown in Figure 5.

III. RESULTS AND DISCUSSIONS

The experimental results for the various laser energies and the focal positions at 4-ms pulse duration are shown in

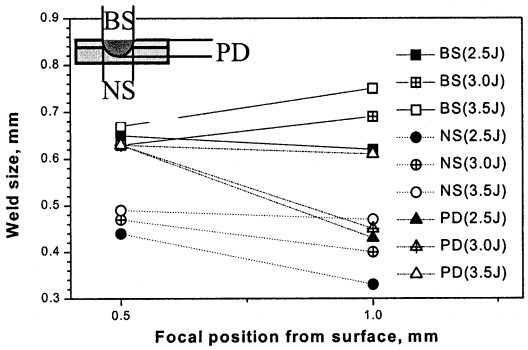

Fig. 6—Experimental results at a pulse duration of 4 ms.

Figure 6. In case of low laser energy, the weld size is smaller as the focal position is further from the surface. But the bead size is enlarged and the penetration depth and nugget size show a slow diminishing trend at high energy. It is considered that the outside of the laser beam which has low beam intensity, is absorbed like surface heat flux, and the inside of the beam which has high beam intensity, creates penetration welding as the focal position is further. So the bead size becomes large by the convection of the molten pool near the surface as the laser energy is higher. And comparing the results for 0.5- and 1-mm focal position, the enlargement of the weld size is minute in the case of 0.5-mm focal position, but the latter shows a remarkable increase of the weld size with increasing power. This is probably due to the fact that the recoil pressure induced by an abrupt rise of temperature in weld part expels the molten metal, and the laser beam with high intensity causes drilling of the plates as focal position is nearer to the surface of specimen, as shown in Figure 5(c). These phenomena reduce the heat transfer by convection of molten metal and make it difficult to calculate the weld shape in thermal analysis. To compare the numerical results of previous models and the proposed one of the heat source equation, the specific condition of laser energy 2.5 J and pulse duration 4 ms, which shows the evident change of weld shape with varying focal position, is applied.

Temperature contours in the workpiece simulated for Eqs. [1] and [2] are shown in Figure 7. For clarity, the contours are presented only in the joint region herein. When Eq. [1] is used, a high temperature occurs near the upper plate of the joint but the melting temperature does not reach the lower plate, which is considered to be the result of a high power beam heating the top surface for a short pulse duration, which is insufficient for heat to transfer by conduction. It shows a very different weld shape from the morphology obtained by experiments. This indicates that considering just conduction by heat flux is not appropriate for predicting the laser-spot-weld shape of thin plates. Conversely, the result using Eq. [2], which treats the laser beam as heat generation in plates from the beginning of pulse duration, shows a low temperature compared to the result using Eq. [1]. The maximum temperature does not even reach the melting point, 1723 K. The absorption coefficient multiplied to power in Eq. [2] weakens the entire power. Therefore, Eq. [2] is appropriate for high-powered CO_2 laser welding of thick plates, which is influenced by plasma in the keyhole.

In the same way, numerical analysis using Eqs. [3] and [4] and the proposed model was performed, and the results

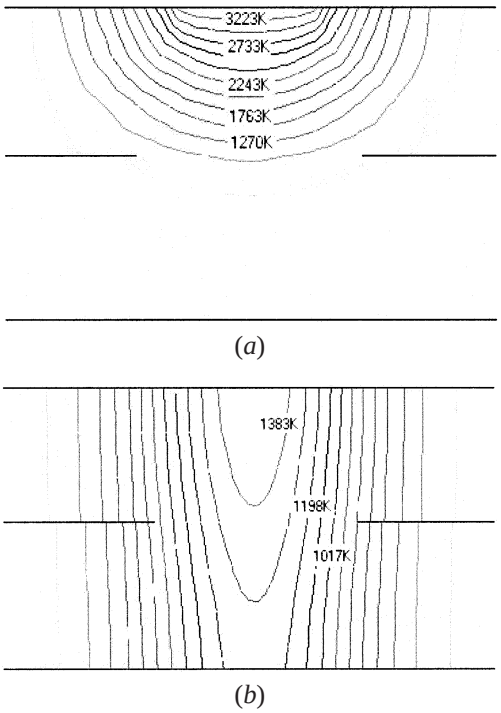

Fig. 7—Calculated results for various heat source equations at a laser energy of 2.5 J and pulse duration of 4 ms: (*a*) Eq. [1] and (*b*) Eq. [2].

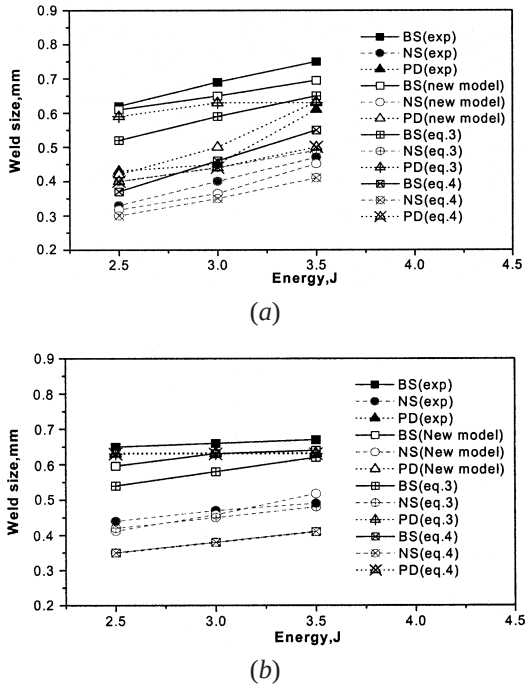

Fig. 9—Comparison of calculated results with the experimental one for various laser energies at a pulse duration of 4 ms: (*a*) focal position: +1.0, and (*b*) focal position: +0.5.

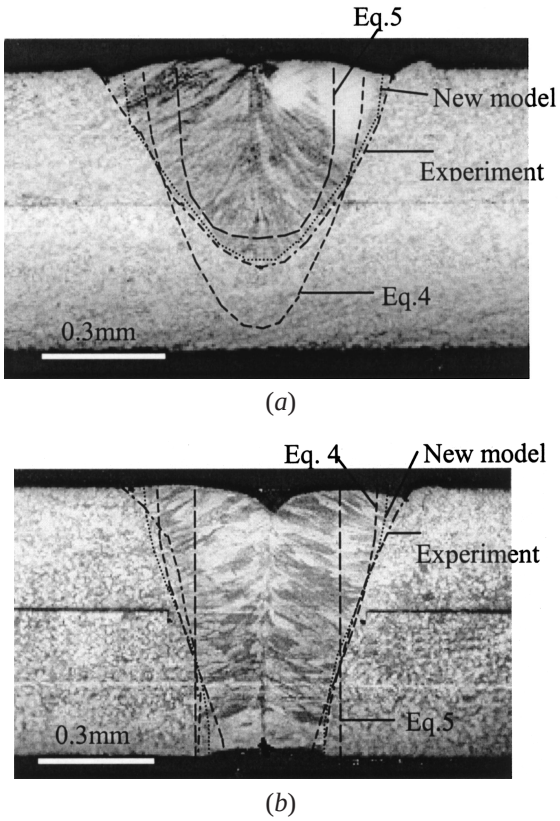

Fig. 8—Comparison of calculated results with the experimental one for various focal positions at energy of 2.5 J and pulse duration of 4 ms: (*a*) focal position: +1.0, and (*b*) focal position: +0.5.

are displayed on the morphology of the sectioned specimen in Figure 8. It shows a typical comparison example of cross sections of experiments and simulations obtained for the thickness combination of 0.3 mm + 0.33 mm with laser energy of 2.5 J and pulse time of 4 ms. In Figure 8(a), the focal point was located 1 mm above the plate, while it was 0.5 mm for the results of Figure 8(b). This micrograph shows that the penetration depth is deeper than the former one, which also appears in numerical results. This comparison has shown that the penetration depth associated with pulsed laser welding is changing drastically as the focal position varies.

The result using Eq. [3] shows a similar weld shape with the experimental one at the 0.5-mm focal position, but it does not reflect the change of the weld shape as the focal position becomes further. Equation [3] does not represent a sensitive change of penetration depth with varying focal position and it gives a narrower bead size than the experimental one. In Eq. [4], the beam penetration depth d_k is calculated iteratively to find the most similar weld shape with the morphology of the sectioned specimen. It is assumed that the laser beam is like the Gaussian rod in penetration welding, so there is no change in weld width from the top surface to the bottom of plates in the case of the 0.5-mm focal position. It also gives a narrow bead size for both of the focal positions. These results, which are obtained by Eqs. [3] and [4], show that there is a limit to predict weld shape for laser spot welding of thin plates. On the other hand, the proposed model, which is modeled to simulate the beam penetration from the surface to the inside of the material, gives fairy well accorded results. It also represents the change of weld shape with varying focal positions. To verify the calculated results, experimental and calculated joint shapes were compared for various welding conditions, as shown in Figures 9. It is shown that the proposed model can predict better than previous models not only the penetration depth and nugget size but also the top bead size well to allow for the

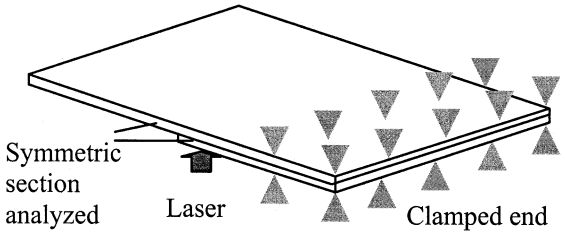

Fig. 10—Boundary conditions for the mechanical analysis.

error in measurement of the sectioned weld parts. From these results, it was shown that the combined model of FEM analysis using the proposed heat source equation could be effectively applied for the prediction of spot weld shape such as penetration depth, nugget size, and top bead size for the thin workpiece pairs.

For verifying the trend of distortion, several mechanical analyses and experiments were performed using the previous heat source equations, which show similar weld shape with the experiment for the lap joint plates. The boundary conditions are shown in Figure 10.

The digital frame memory for measurement has a relatively high input rate of 1/15 sec for each frame. Taking advantage of this fact, transient shape change of the laser-welded plate has been investigated by using ESPI. Some typical fringe patterns obtained are shown in Figure 11(a), and the number of fringes is calculated in a specific time and the numerical results displayed in Figure 11(b) to show the displacement history. It shows clearly that, among various heat source models considered, the results of measurement are in the best agreement with the results obtained by using the new model adopted in this study.

IV. CONCLUSIONS

From the results of finite-element analysis for laser spot welding of thin stainless steel sheets, the following conclusions may be drawn.

1. To simulate the laser spot welding, which is sensitively affected by process parameters, the heat source equation reflecting the real phenomena is required.
2. The FEM using the proposed heat source equation can estimate the laser spot weld bead shape of thin stainless steel sheets more precisely than the previously used ones.
3. The proposed heat source equation can predict the laser-spot-weld bead shape of thin stainless steel sheets with varying process parameters such as focal position and laser energy well.
4. Precise thermal analysis using the proposed heat source equation could be effectively used to analyze the mechanical attributes of the small structure joint, *i.e.*, the thermal distortion and residual stresses.

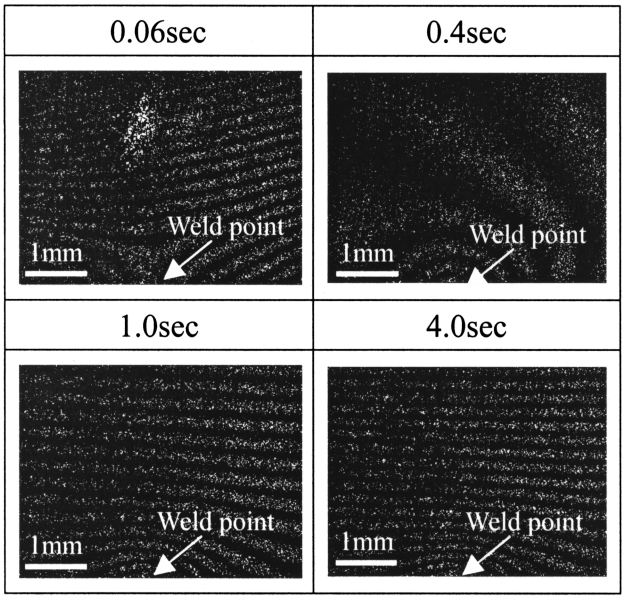

(*a*)

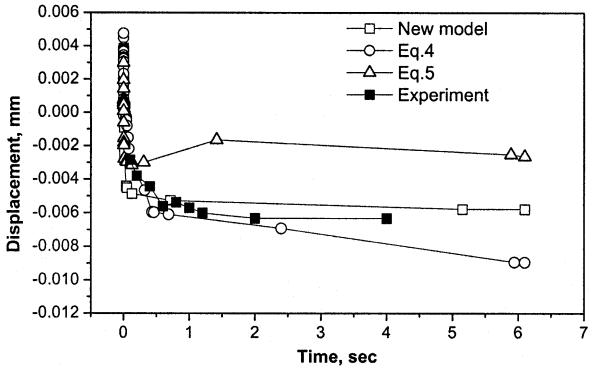

(*b*)

Fig. 11—Typical fringe patterns and comparison of displacement history at the end of the plate in the *z* direction with varying heat source equations. (*a*) Fringe patterns on the lap welded plates. (*b*) Comparison of results.

NOMENCLATURE

$P(t)$	time-dependent laser power (W)
$\rho(T)$	temperature-dependent density (kg m^{-3})
$C(T)$	temperature-dependent specific heat capacity (J kg^{-1} K^{-1})
$K(T)$	temperature-dependent thermal conductivity (W m^{-1} K^{-1})
Q	power generation per unit volume in the domain (W m^{-3})
k_n	thermal conductivity normal to surfaces that are subject to radiation, convection, and imposed heat fluxes (W m^{-1} K^{-1})
q	heat flux (W m^{-2})
h	heat-transfer coefficient for convection (W m^{-2} K^{-1})
σ	Stefan–Boltzmann constant for radiation (W m^{-2} K^{-4})
ε	emissivity
T_{Sol}	solidus temperature (K)
T_{Liq}	liquidus temperature (K)

REFERENCES

1. D. Rosenthal: *Trans. ASME*, 1946, vol. 43, pp. 849-66.
2. W. M. Steen, J. Dowden, M. Davis, and P. Kapadia: *J. Phys. D: Appl. Phys.*, 1988, vol. 21, pp. 1255-60.
3. J. Mazumder and W.M. Steen: *J. Appl. Phys.*, 1980, vol. 51, pp. 941-47.

4. T. Zacharia, S.A. David, J.M. Vitek, and T. DebRoy: *Weld. J.*, 1989, vol. 68, pp. 499s-509s.
5. T. Zacharia, S.A. David, J.M. Vitek, and T. DebRoy: *Metall. Mater. Trans. A*, 1989, vol. 20A, pp. 957-67.
6. J.D. Kim: *KSME J.*, 1990, vol. 4, pp. 32-39.
7. O.O.D. Neto and C.A.S. Lima: *J. Phys. D: Appl. Phys.*, 1994, vol. 27, pp. 1795-1804.
8. N. Sonti and M.F. Amateau: *Num. Heat Transfer*, 1989, vol. 16A, pp. 351-70.
9. R. Mueller: *Proc. ICALEO '94*, 1994, pp. 509-18.
10. H. Hügel: *Strahlwerkzeug Laser*, Teubner, Stuttgart, 1992.
11. V.V. Semak and A. Matsunawa: *J. Phys. D: Appl. Phys.*, 1997, vol. 30, pp. 2541-52.
12. V.V. Semak, B. Damkroger, and S. Kempka: *J. Phys. D: Appl. Phys.*, 1999, vol. 32, pp. 1819-25.
13. S.I. Anisimov and V.A. Khoklov: *Instabilities in Laser-Matter Interaction*, CRC Press, Boca Raton, FL, 1995.
14. M.R. Frewin and D. A. Scott: *Weld. J.*, 1999, vol. 78, pp. 15s-22s.
15. Y. Matsuhiro, Y. Inaba, and T. Ohji: *Jpn. Weld. Soc.*, 1993, vol. 11, pp. 479-83.
16. W.M. Steen: *Laser Material Processing*, Springer-Verlag, New York, NY, 1991.
17. A. Kaplan: *J. Phys. D: Appl. Phys.*, 1994, vol. 27, pp. 1805-14.
18. P. Tekriwal and J. Mazumder: *Weld J.*, 1988, vol. 67, pp. 150s-156s
19. J. Wilson and J.F.B. Hawkes: *Lasers: Principles and Applications*, Prentice-Hall, Englewood Cliffs, NJ, 1987.
20. *ABAQUS Theory Manual*, Version 5.4, Hibbitt, Kalsson & Sorensen, Inc., Pawtucket, RI, 1994.
21. M. Sjödahl: *Optics Lasers Eng.*, 1998, vol. 29, pp. 125-44.
22. N.K. Mohan, H. Saldner, and N.E. Molin: *Optics Lett.*, 1993, vol. 18, pp. 1861-63.